Journal of Materials Chemistry C

PAPER

View Article Online
View Journal | View Issue

Cite this: J. Mater. Chem. C, 2018, 6, 6153

Monolayer tellurene–metal contacts

Jiahuan Yan, †[a] Xiuying Zhang, †[a] Yuanyuan Pan,[a] Jingzhen Li,[a] Bowen Shi,[a] Shiqi Liu,[a] Jie Yang,[a] Zhigang Song,[a] Han Zhang,[a] Meng Ye,[a] Ruge Quhe,[b] Yangyang Wang,[c] Jinbo Yang,[ad] Feng Pan*[e] and Jing Lu*[ad]

Received 26th March 2018,
Accepted 9th May 2018

DOI: 10.1039/c8tc01421c

rsc.li/materials-c

Two-dimensional (2D) atomic crystals are promising channel materials for next generation electronics due to its outstanding gate electrostatics and few dangling bonds. Recently, tellurene, a new experimentally accessible Group-VI 2D tellurium, has drawn attention due to its large on/off ratios, high mobility and significant air stability. Herein, for the first time, we comprehensively examine the interfacial characteristics of monolayer (ML) tellurene field-effect transistors with a series of common bulk metals and 2D graphene as electrodes by using *ab initio* electronic structure calculations and quantum transport simulations. Furthermore, a lateral n-type Schottky contact is formed when contacting with Au in the *a* direction and Sc in both directions, while a lateral p-type Schottky contact is formed with Au in the *b* direction, and Cu, Ni, Ag, Pt, and Pd in both directions as a result of strong Fermi level pinning (FLP). The obtained FLP factor is 0.15 in the *a* direction and 0.09 in the *b* direction. Remarkably, a highly desirable lateral p-type Ohmic contact is formed with graphene in both directions. This investigation gives insight into the interfacial properties and guidance in electrode selection for ML tellurene devices.

Introduction

Two-dimensional (2D) semiconductors have the advantage of outstanding gate controllability due to their atomic thickness and few interface traps owning to their dangling-bond-free interface, and thus are promising channel material candidates for next generation electronic and optoelectronic devices.[1–3] Recently, Group-VI tellurene (2D tellurium Te), a new member of the 2D semiconductor family, has been experimentally attained.[4–7] Anisotropic tellurene consists of tetragonal and hexagonal rings (Fig. 1a).[8,9] The band gap of tellurene is from nearly direct 0.33 eV (in the bulk) to indirect 0.92 eV (monolayer (ML)).[4,6,9–13] Tellurene field effect transistors (FET) experimentally show a large on/off ratio of 10^6 and a high mobility of up to 700 cm^2 $(V\ s)^{-1}$,[6] the latter of which is higher than that of MoS_2[14–16] and $MoSe_2$.[17–20] Furthermore, tellurene has significant air stability compared with the air-sensitive black phosphorene.[6,21,22] Above all, these superiorities allow tellurene to join the competitive 2D channel material rank.

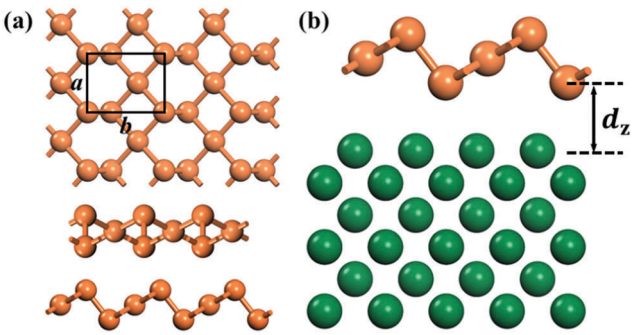

Fig. 1 (a) Top- and side-views of free-standing ML tellurene. (b) Initial configuration of ML tellurene on the metal surface (green balls).

In a practical 2D semiconductor device, the conventional doping method usually is substituted by a direct contact with a metal to inject carriers due to the deficiency of sustainable and controllable substitutional doping methods for 2D materials.[23,24] However, such direct contact induces the formation of a Schottky barrier in semiconductor–metal junctions due to the Fermi level pinning (FLP) derived from the interaction between the electrode and channel, which reduces the carrier injection efficiency and then depresses the device performance.[24,25] Therefore, it is important to form low contact resistance by decreasing the Schottky barrier height (SBH) to reveal the prominent intrinsic

[a] State Key Laboratory for Mesoscopic Physics and Department of Physics, Peking University, Beijing 100871, P. R. China. E-mail: jinglu@pku.edu.cn
[b] State Key Laboratory of Information Photonics and Optical Communications and School of Science, Beijing University of Posts and Telecommunications, Beijing 100876, P. R. China
[c] Nanophotonics and Optoelectronics Research Center, Qian Xuesen Laboratory of Space Technology, China Academy of Space Technology, Beijing 100094, P. R. China
[d] Collaborative Innovation Center of Quantum Matter, Beijing 100871, P. R. China
[e] School of Advanced Materials, Peking University, Shenzhen Graduate School, Shenzhen 518055, China. E-mail: panfeng@pkusz.edu.cn
† These authors contributed equally to this work.

properties of 2D materials. Obviously, prediction of the SBH is desirable for the development of tellurene devices. Experimentally, tellurene transistors have been fabricated with Ni and Pd/Au as electrodes.[6] However, a comprehensive examination of the interfacial properties between ML tellurene and common metals remains scarce.

Herein, for the first time, we systematically examine the interfacial characteristics of ML tellurene with 2D graphene and metal (Sc, Ag, Cu, Au, Ni, Pt, and Pd) electrodes spanning a wide work function range in a transistor configuration by using *ab initio* electronic structure calculations and quantum transport simulations. The band structures of ML tellurene contacted with bulk metals are heavily hybridized and ML tellurene undergoes metallization, which means no SBH exists in the vertical direction. Differently, there is still a band gap when ML tellurene is placed on top of the 2D graphene surface, and a vertical p-type Ohmic contact is shaped. A lateral n-type Schottky contact is shaped between ML tellurene and Au in the *a* direction (with a lateral electron SBH of 0.44 eV) and Sc in both *a* and *b* directions (with a lateral electron SBH of 0.30 eV and 0.41 eV, respectively). In contrast, a lateral p-type Schottky contact is shaped when contacting with Au in the *b* direction (with a lateral hole SBH of 0.43 eV) and Cu, Ni, Ag, Pt, and Pd in both *a* and *b* directions (with a lateral hole SBH of 0.45, 0.37, 0.37, 0.28, and 0.20 eV in the *a* direction and 0.32, 0.42, 0.30, 0.27, and 0.28 eV in the *b* direction, respectively). The formation of the lateral Schottky barrier stems from the strong FLP caused by the metal-induced gap states (MIGS), where the pinning factors are 0.15 and 0.09 in the *a* direction and *b* direction, respectively. Remarkably, a highly desirable lateral p-type Ohmic contact is formed with graphene in both directions owing to the match of the work function of ML graphene with the valence band maximum (VBM) of ML tellurene and weak FLP at the interface.

Computational details

The optimized in-plane lattice constants of ML tetragonal tellurene are a = 4.19 Å and b = 5.49 Å, which are in good accordance with the previously computed results.[8,9] We chose seven metals (Sc, Ag, Cu, Au, Ni, Pt, and Pd) as electrodes because they cover a wide work function range from 3.58 to 5.65 eV. Besides, experimentally, these metals are commonly used as electrodes in FETs,[26] and tellurene transistors with Ni and Pd/Au as electrodes have been fabricated.[6] We employed six layers of metal atoms to simulate the metal surface because six-layer metal atoms are sufficient to characterize a real metal substrate according to the convergence tests carried out in previous studies.[27–31] The bottom three layers of the metal atoms were fixed because ML tellurene interacts mainly with the top layers. Moreover, we adjusted the lattice constants of the metals and ML graphene to match that of ML tellurene. We adapted a 1×2 Au(110)/Ag(110) supercell and $\sqrt{3} \times 2$ Cu(111)/Ni(111)/ML graphene supercell to an $a \times b$ ML tellurene supercell and $4 \times \sqrt{3}$ Sc(0001)/Pt(111)/Pd(111) supercell to a $3a \times b$ ML tellurene supercell. The corresponding mismatches of the lattice constant are within 5%, as shown in Table 1. A vacuum buffer space of more than 15 Å was set to avert pseudo interaction.

Table 1 Calculated interlayer properties of ML tellurene–metal contacts. $\bar{\varepsilon}$ is the average lattice constant mismatch between the metal surface and ML tellurene. The equilibrium distance d_z is the average distance between the contact ML tellurene–metal interfaces in the vertical direction. $d_{\mathrm{Te-M}}$ is the minimum atom-to-atom distance from the tellurene atom to the metal atom. The binding energy, E_b, is the energy per tellurium atom to remove ML tellurene from the metal surface. W_M and $W_{\mathrm{Te-M}}$ are the calculated WF for a clean metal surface and the ML tellurene–metal system, respectively. $\Phi^{e}_{L,W}$ ($\Phi^{h}_{L,W}$) is the electron (hole) SBH obtained from the WFA in the lateral direction. $\Phi^{e,a}_{L,T}$ and $\Phi^{e,b}_{L,T}$ ($\Phi^{h,a}_{L,T}$ and $\Phi^{h,b}_{L,T}$) are the electron (hole) transport SBHs obtained from the quantum transport simulation in the lateral *a* direction and *b* direction, respectively. E^{a}_{g} and E^{b}_{g} are the transmission gaps in the *a* direction and *b* direction, respectively

Metal	Sc	Au	Cu	Ni	Ag	Pt	Pd	Graphene
$\bar{\varepsilon}$ (%)	3.23	2.35	4.40	4.51	2.35	3.27	3.60	4.57
d_z (Å)	2.47	1.78	1.95	1.76	1.48	2.20	2.15	3.55
$d_{\mathrm{Te-M}}$ (Å)	2.76	2.84	2.51	2.39	2.82	2.57	2.53	3.82
E_b (eV)	3.00	1.76	2.23	3.04	1.86	3.33	3.36	0.23
W_M (eV)	3.58	4.96	4.60	5.01	4.19	5.65	5.12	4.58
$W_{\mathrm{Te-M}}$ (eV)	3.81	4.52	4.45	4.50	4.24	4.87	4.62	4.55
$\Phi^{e}_{L,W}$ (eV)	0.34	1.05	0.98	1.02	0.77	1.40	1.15	1.08
$\Phi^{h}_{L,W}$ (eV)	0.80	0.10	0.17	0.12	0.37	−0.26	−0.01	0.06
$\Phi^{e,a}_{L,T}$ (eV)	0.30	0.44	0.58	0.62	0.59	0.69	0.80	1.00
$\Phi^{h,a}_{L,T}$ (eV)	0.67	0.54	0.45	0.37	0.37	0.28	0.20	0
$\Phi^{e,b}_{L,T}$(eV)	0.41	0.53	0.70	0.58	0.70	0.74	0.69	0.97
$\Phi^{h,b}_{L,T}$ (eV)	0.57	0.43	0.32	0.42	0.30	0.27	0.28	0
E^{a}_{g} (eV)	0.97	0.98	1.03	0.99	0.96	0.97	1.00	1.00
E^{b}_{g} (eV)	0.98	0.96	1.02	1.00	1.00	1.01	0.97	0.97

When performing the geometry optimizations and electronic structure calculations, we used the projector-augmented wave (PAW) pseudopotential[32,33] and plane-wave basis set with a cut-off energy of 400 eV, as implemented in the Vienna *ab initio* simulation package (VASP).[34–37] The stopping criterion of the geometry optimizations was the residual force below 0.01 eV Å^{-1} on each atom. For all the calculated structures, the Monkhorst–Pack *k*-point $5 \times 5 \times 1$ mesh was sampled for the structural optimizations and $9 \times 9 \times 1$ for electronic structure calculations in the Brillouin zone.[38] Also, we took two corrections into account. One is the van der Waals (vdW) interaction with the zero damping DFT-D3 method of Grimme,[39] and other is the dipole correction, which is applied to eliminate the pseudo interaction of the dipole moments caused by periodicity in the *z*-direction.

A two-probe model was constructed to simulate an FET with a 5 nm channel of ML tellurene and electrodes made of optimized ML tellurene–metal/graphene interfaces, as shown in Fig. 5. The right and left electrodes are semi-infinite. The local device density of states (LDDOS) and the transmission spectra were calculated using the density functional theory coupled with the non-equilibrium Green's function (NEGF) method implemented in the Atomistix ToolKit (ATK) 2016 package.[40–44] The transmission coefficient $T^{k_{||}}(E)$ ($k_{||}$ is a reciprocal lattice vector point along a surface-parallel direction (orthogonal to the transmission direction) in the irreducible Brillouin zone (IBZ)) is calculated as:

$$T^{k_{||}}(E) = \mathrm{Tr}\left[\Gamma_{\mathrm{L}}^{k_{||}}(E) G^{k_{||}}(E) \Gamma_{\mathrm{R}}^{k_{||}}(E) G^{k_{||}\dagger}(E)\right]$$

where, $\Gamma_{L/R}^{k_{||}}(E) = i\left(\Sigma_{L/R}^{r,k_{||}} - \Sigma_{L/R}^{a,k_{||}}\right)$ stands for the level broadening induced by the left electrodes and the right electrodes appearing in the form of the electrode self-energies $\Sigma_{L/R}^{k_{||}}$, which is a reflex of the impact of the electrodes on the scattering region.[45] $G^{k_{||}}$ and $G^{k_{||}\dagger}$ is the retarded and advanced Green's function, respectively. The average of $T^{k_{||}}(E)$ over different $k_{||}$ in the IBZ gives the transmission function at a given energy $T(E)$. A double-ξ polarized (DZP) basis set was employed. The temperature was set at 300 K and the real-space mesh cutoff was 75 Hartrees. The electronic structures of the electrodes and central region were calculated with a Monkhorst–Pack[38] of 50 × 1 × 50 and 50 × 1 × 1 k-point grids, respectively. A Dirichlet type, Neumann type and periodic type boundary condition[46] were used in the z-, y- and x-directions of the device (see Fig. 7), respectively. Additionally, the generalized gradient approximation (GGA) functional to the exchange-correction functional of the Perdew–Burke–Ernzerhof (PBE) form[47] was employed throughout.

Since the 2D semiconductor channel is doped by carriers from the metal electrodes and the electron–electron interaction is strongly restrained, the single electron approximation is effective to describe the electron behavior in an FET configuration; thus we chose the DFT-GGA to evaluate the SBH.[48,49] For example, the theoretical transport gap of ML, bilayer (BL), and trilayer (TL) black phosphorene with an Ni electrode at the DFT-GGA level is 0.65, 0.81 and 0.68 eV,[28,50,51] respectively, which is in accordance with the experimental values (0.99, 0.71 and 0.61 eV for ML, BL and TL,[26] respectively). Obviously, the DFT-GGA method provides the optimal calculated value. In addition, in the ML/BL/TL phosphorene FET with an Ni electrode, the calculated hole (electron) SBH with the DFT-GGA method is 0.26/0.19/0.20 (0.39/0.52/0.48) eV,[28,50,51] which is in excellent accordance with the observed value of 0.35/0.23/0.21 (0.64/0.48/0.40) eV.[26]

Results and discussion

ML tellurene–metal/graphene interface

After structural optimization, the structure of ML tellurene changes slightly on the Sc, Au, Cu, Ni, Ag and graphene surfaces, while strongly on the Pt and Pd surfaces, as shown in Fig. 2. The equilibrium distance, d_z, is the vertical average distance between ML tellurene and the closest metal layer, as shown in Fig. 1(b), and d_{Te-M} is the minimum atomic distance between the tellurene atom and the metal atom. The binding energy, E_b, of the ML tellurene–metal/graphene system is defined as:

$$E_b = (E_{Te} + E_M - E_{Te-M})/N$$

where, E_{Te}, E_M and E_{Te-M} are the relaxed energy of the pure ML tellurene, pure metal/graphene surface and ML tellurene–metal/graphene systems, respectively, and N is the number of tellurene atoms contacted directly with the metal. The relevant parameters of the ML tellurene–metal/graphene system are listed in Table 1.

According to the binding energy, E_b, the interactions between ML tellurene and metal/graphene surface can be divided into three groups. The first is ML tellurene on ML graphene with weak vdW interaction, which is characterized by the smallest E_b (0.23 eV) and the largest distance d_z (3.55 Å) and d_{Te-M} (3.82 Å) among all the contacts. The second is ML tellurene on Au, Ag and Cu surfaces with moderate adhesion, which features a slightly large E_b (1.76–2.23 eV) and small d_z (1.48–1.95 Å) and d_{Te-M} (2.51–2.84 Å). The third group is ML on Sc, Ni, Pt and Pd surfaces with strong adhesion, which is characterized by a quite large E_b (3.00–3.36 eV) and small d_z (1.76–2.47 Å) and d_{Te-M} (2.39–2.76 Å).

The differences between the bond strength in the latter two groups are ascribed to the different numbers of unpaired electrons. Free-standing Au ($5d^{10}6s^1$), Ag ($4d^{10}5s^1$) and Cu ($3d^{10}4s^1$) atoms have one unpaired electron in their outermost orbital, accompanied by one covalent bond with ML tellurene. Thus, a relative small

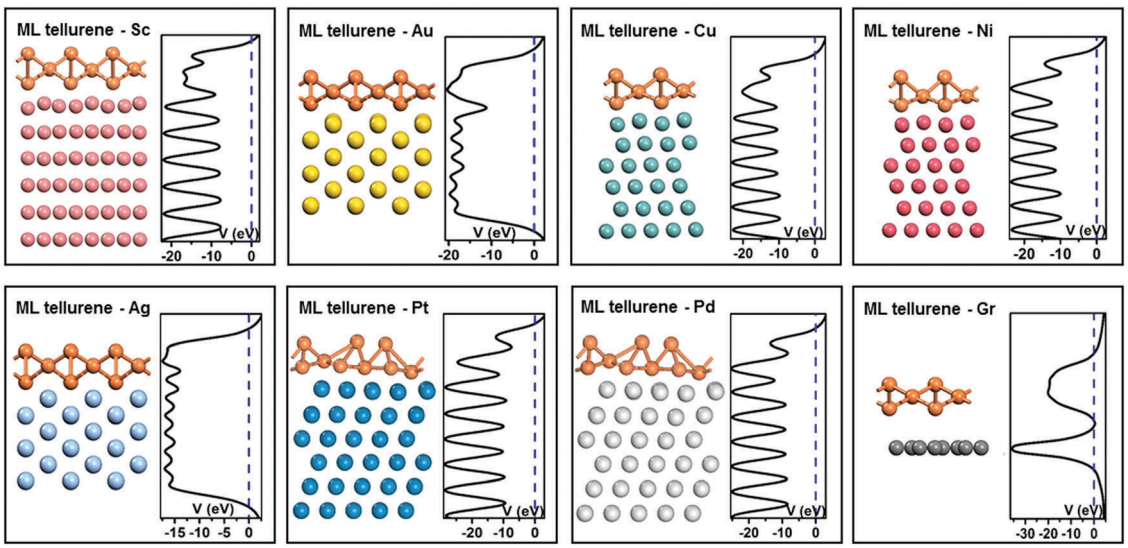

Fig. 2 Side-view of the optimized structure and average electrostatic potential distribution in the planes normal to the interface of ML tellurene on Sc, Au, Cu, Ni, Ag, Pt, Pd and graphene surfaces. The Fermi level is set to zero and denoted by the blue dashed lines.

binding energy is obtained with ML tellurene. Free-standing Ni ($3d^8 4s^2$) and Pt ($5d^9 6s^1$) atoms both have two unpaired electrons and form two covalent bonds with ML tellurene. Free-standing Pd ($4d^{10}$) and Sc ($3d^1 4s^2$) atom have zero and one unpaired electron, respectively. However, according to the Mulliken population analysis, the Pd and Sc atoms have approximately two and three unpaired electrons ($4d^9 5s^1$ for Pd and $3d^1 4s^1 4p^1$ for Sc), respectively, when they are contacted with tellurene because hybridization occurs between the 4d and 5s orbitals of Pd atom and between the 3d, 4s and 4p orbitals of Sc atom owing to the overlap of the d orbital with broadened s and p orbitals. Thus, the Pd and Sc atoms form two and three covalent bonds with ML tellurene, respectively. Thus, the Pd, Sc, Ni and Pt atoms have large binding energies with ML tellurene.

The band structures of the free-standing ML tellurene and ML tellurene–metal/graphene systems are shown in Fig. 3. ML tellurene has an indirect band gap of 1.14 eV without spin-orbital coupling, which is in good accordance with the previous DFT result of 1.17 eV.[8] The band structures of ML tellurene are strongly destroyed on all the metal surfaces, which suggests a covalent interaction between ML tellurene and all the investigated metals. The hybridization degree of the band structure is much stronger when ML tellurene on the Sc, Ni, Pt and Pd surfaces than on the Au, Ag and Cu surfaces owing to more covalent bonds. Besides, some bands of ML tellurene on all the metal surfaces always cross the Fermi level, suggesting the metallization of ML tellurene. In contrast, the band structure of ML tellurene is preserved well on the graphene surface due to weak vdW interactions.

The partial density of states (PDOS) of the free-standing ML tellurene and ML tellurene–metal/graphene surfaces are shown in Fig. 4. The band gap disappears for ML tellurene on all the checked metal surfaces as a result of the hybridization of the band structure and the metallization of ML tellurene. There is a clear band gap of ML tellurene on the graphene surface, which is in great accordance with the weak vdW interactions achieved previously at the interface. The Fermi level is dominated by the p orbital of ML tellurene.

ML tellurene transistors

A schematic diagram of an ML tellurene transistor is shown in Fig. 5. The Schottky barrier depresses the electron transport and degrades the performance of an FET. There are two types of interfaces possibly present in the Schottky barrier in an ML tellurene transistor. One is a vertical Schottky barrier (Φ_V) at the interface A (between the ML tellurene and metal/graphene surface) in the vertical direction. The other is a lateral Schottky barrier (Φ_L) at interface B (between the ML tellurene channel and electrode) in the lateral a (b) direction. The lateral SBHs in both methods are shown in Table 1 and Fig. 8.

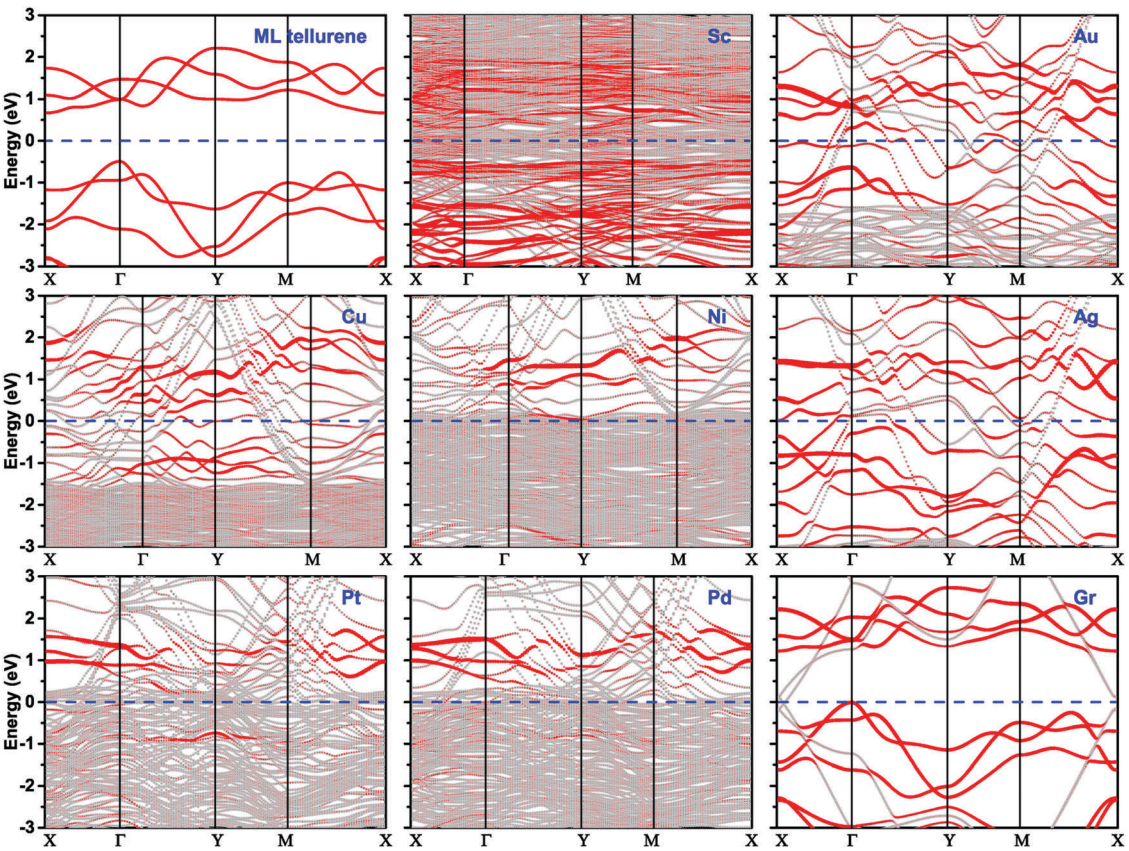

Fig. 3 Band structures of ML tellurene and the ML tellurene–metal systems (projected to the ML tellurene). Gray line: band structure of the interfacial systems; and red line: band structures projected to the ML tellurene. The Fermi level is set at zero energy and denoted by the blue dashed lines.

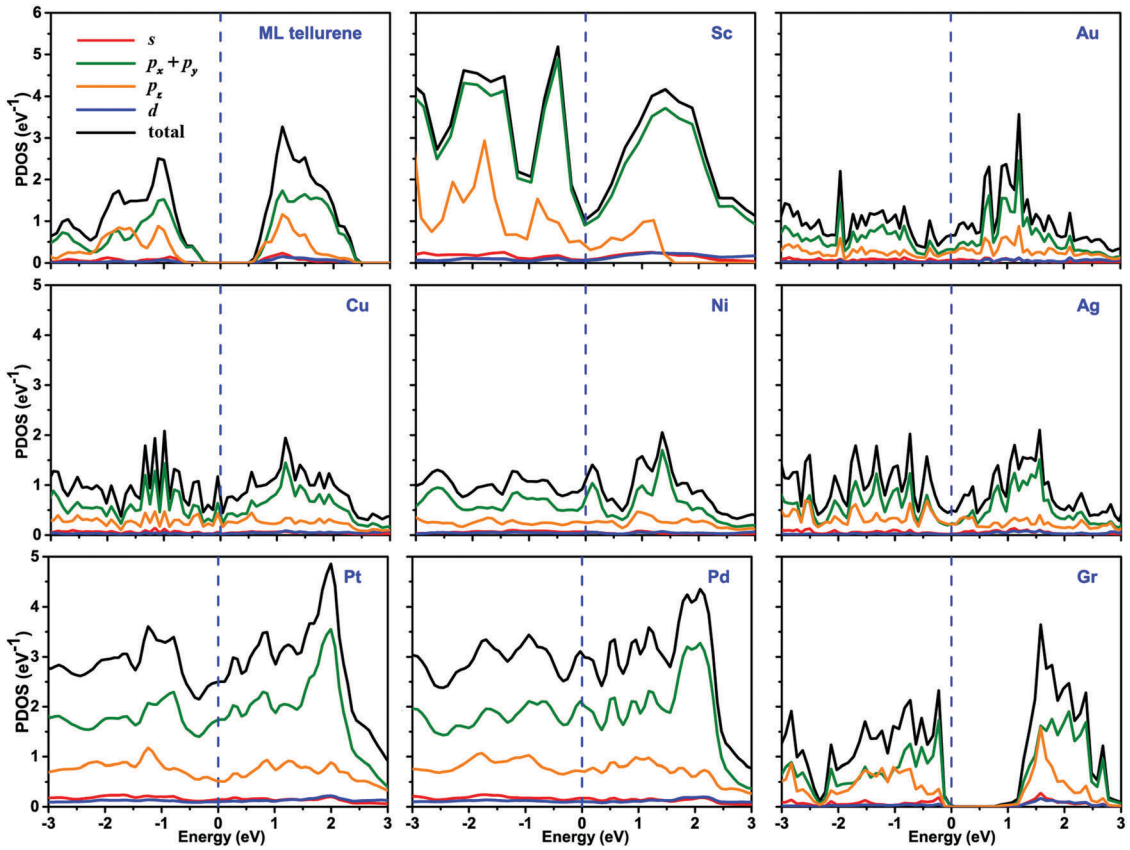

Fig. 4 Partial density of states (PDOS) of ML tellurene and ML tellurene on the metal surfaces from the energy band calculations. The Fermi level is set at zero energy and denoted by the vertical blue dashed lines.

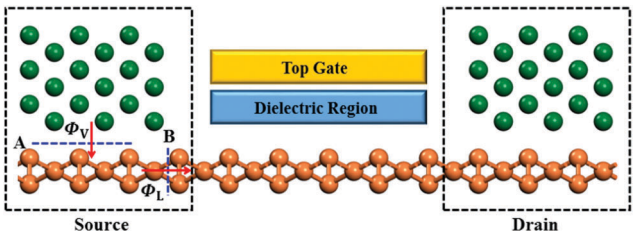

Fig. 5 Schematic diagrams of ML tellurene FETs. Blue dashed lines denote the interfaces where Schottky barriers may exist. Φ_V and Φ_L represent the vertical SBH and lateral SBH, respectively. Red rows represent the pathways that the electrons or holes transfer through the interfaces shown in blue dashed lines.

Φ_V is defined as the difference between the Fermi level and conduction band minimum (CBM)/VBM at the interface A (Fig. 5), which can be attained from the band structures of the ML tellurene–metal/graphene interfaces (Fig. 3) or the LDDOS of ML tellurene transistors at the electrode (Fig. 6 and 7). The metallization of ML tellurene on the seven metal surfaces leads to the absence of a vertical Schottky barrier. On the other hand, the band structure of ML tellurene on the graphene surface is preserved well. The Fermi level crosses the valence band of ML tellurene because the work function of intrinsic ML graphene (4.58 eV) is close to the VBM of intrinsic ML tellurene (4.61 eV). Therefore, the vertical hole SBH (Φ_V^h) is zero, resulting in a vertical p-type Ohmic contact on the graphene surface.

Φ_L is attained from two methods, the work function approximation (WFA) and more accurate quantum transport simulation. The lateral electron (hole) SBH at the WFA level $\Phi_{L,W}^{e(h)}$ is defined as the difference between the Fermi level of the ML tellurene–metal/graphene structure and CBM (VBM) of pure ML tellurene. This method neglects the interaction between the channel ML tellurene and metal/graphene electrode. In the WFA method, a lateral n-type Schottky contact is only formed with the Sc electrode with the lateral electron SBH ($\Phi_{L,W}^e$) of 0.34 eV. A lateral p-type Schottky contact is formed with the Au, Cu, Ni, Ag and graphene electrodes with the lateral hole SBH ($\Phi_{L,W}^h$) of 0.10, 0.17, 0.12, 0.37 and 0.06 eV, respectively. Furthermore, a lateral p-type Ohmic contact is formed with Pt and Pd.

The lateral electron (hole) SBH at the quantum transport simulation level $\Phi_{L,T}^{e(h)}$ is defined as the difference between the Fermi level and the CBM/VBM at the lateral interface B (Fig. 5), which can be attained from the LDDOS of ML tellurene transistors. The LDDOS and transmission spectra of the ML tellurene transistors are depicted in Fig. 6 and 7. The quantum transport simulation method provides a more accurate SBH value than the WFA method because it takes into account the interaction between the channel ML tellurene and metal/graphene electrode. This interaction leads to FLP, which enhances the difficulty of forming a lateral Ohmic contact.

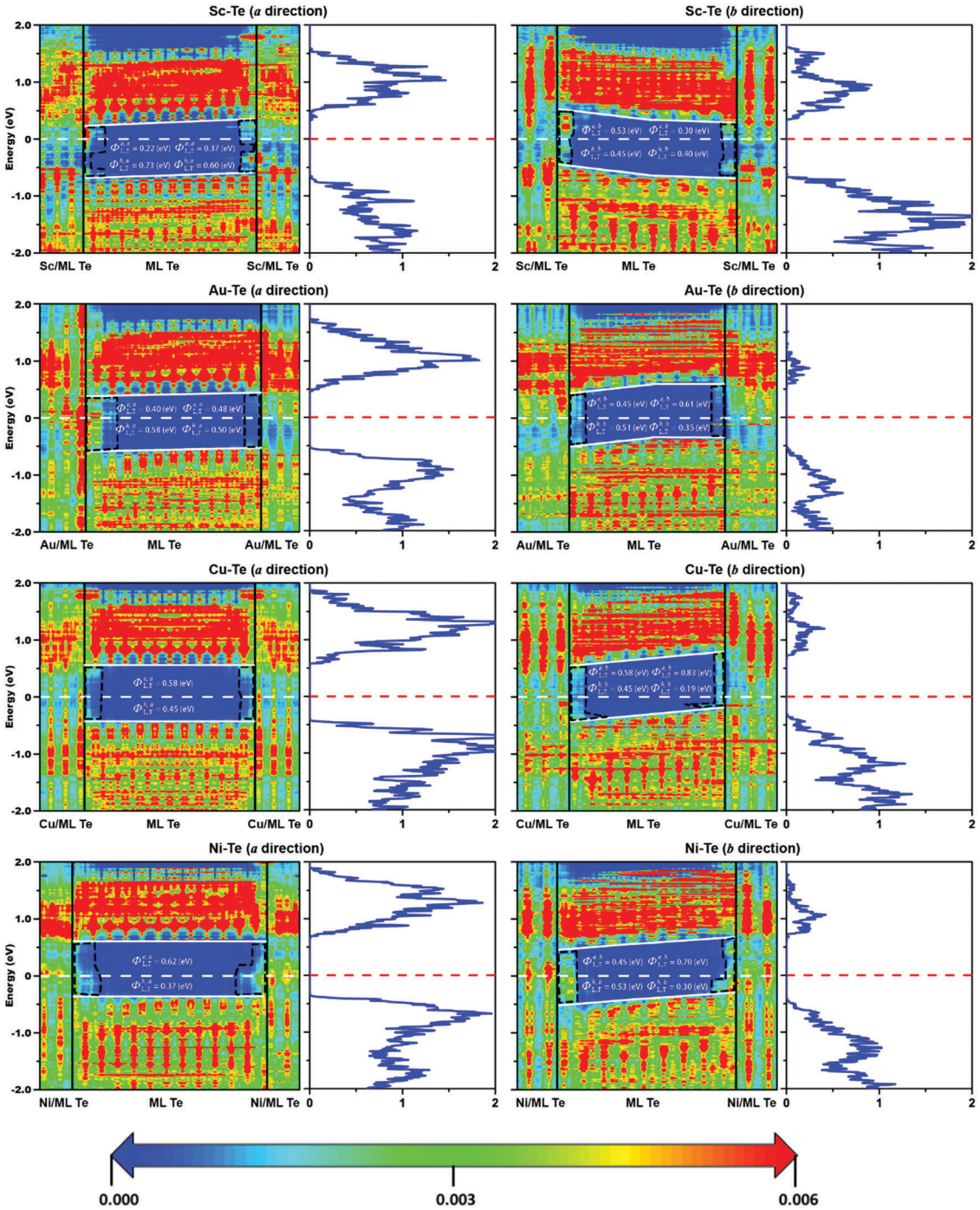

Fig. 6 Zero-bias and zero-gate voltage LDDOS (left panel) and transmission spectra (right panel) of the ML tellurene FETs with Sc, Au, Cu and Ni electrodes, and a channel length of L = 5 nm. $\Phi_{L,T}^{e,a}$ ($\Phi_{L,T}^{e,b}$) and $\Phi_{L,T}^{h,a}$ ($\Phi_{L,T}^{h,b}$) represent the electron SBH and hole SBH in the lateral a (b) direction, respectively. The Fermi level is represented by the white and red dashed lines, respectively. The MIGS are circled by a black dashed line. The color scale is shown below the plot.

In the quantum transport simulation, due to the anisotropy of tellurene, we calculated the transport properties of the ML tellurene FETs along both a and b directions, as shown in Fig. 1(a). In the case of asymmetrical left and right electrodes, we took the average of the lateral SBHs at left and right interfaces. In the a direction, a lateral n-type Schottky contact is formed with Sc and Au with the lateral electron SBH ($\Phi_{L,T}^{e,a}$) of 0.30 and 0.44 eV, respectively. In contrast, a lateral p-type Schottky contact is formed with Pd, Pt, Ni, Ag and Cu with the lateral hole SBH ($\Phi_{L,T}^{h,a}$) of 0.20, 0.28, 0.37, 0.37 and 0.45 eV in the same direction, respectively. In the b direction, a lateral n-type Schottky contact is only formed with Sc with the lateral electron SBH ($\Phi_{L,T}^{e,b}$) of 0.41 eV. In contrast, a lateral p-type Schottky contact is formed with Pt, Pd, Ag, Cu, Ni and Au with the lateral hole SBH ($\Phi_{L,T}^{h,b}$) of 0.27, 0.28, 0.30, 0.32, 0.42 and 0.43 eV in the b direction, respectively. Strikingly, a lateral p-type

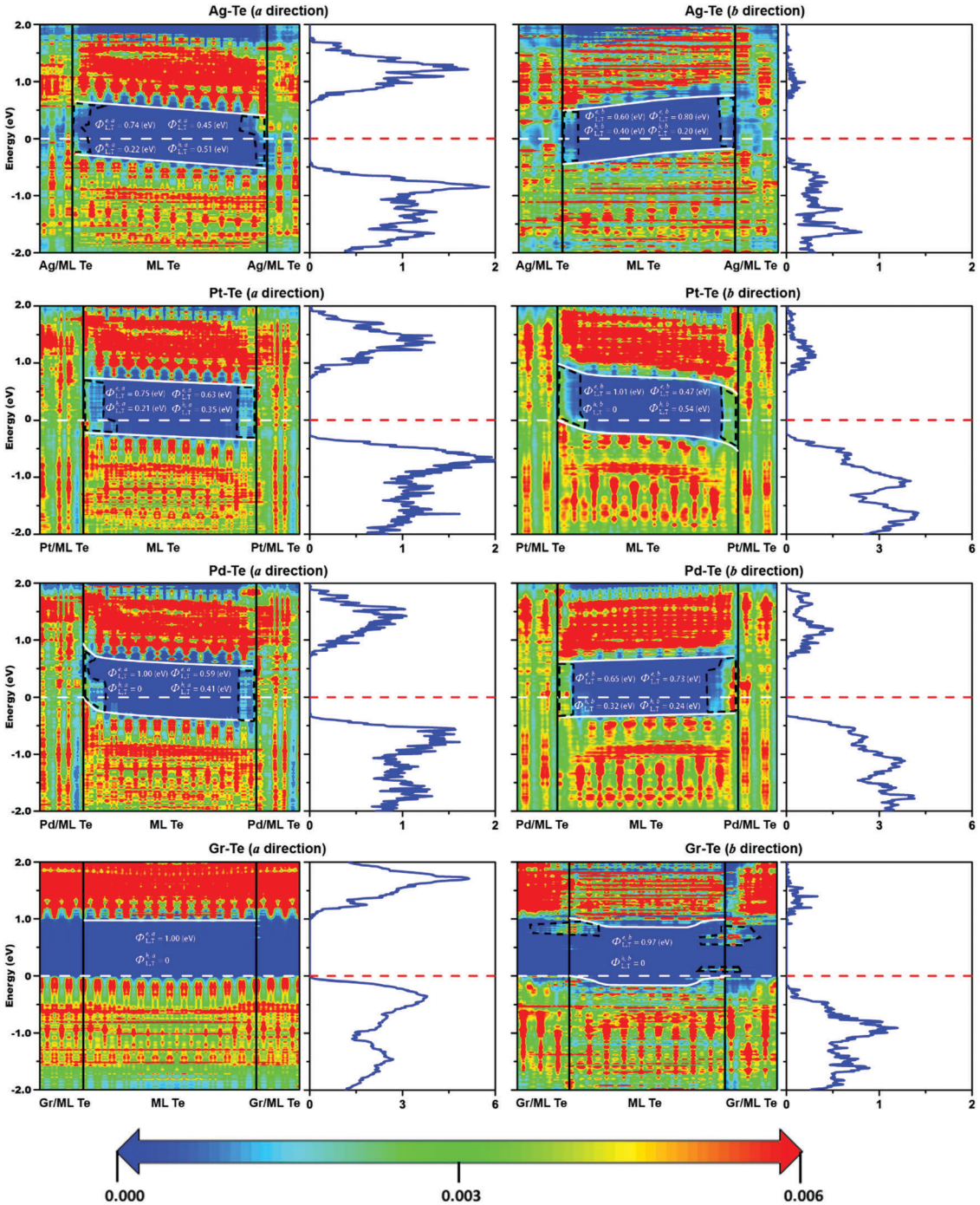

Fig. 7 Zero-bias and zero-gate voltage LDDOS (left panel) and transmission spectra (right panel) of the ML tellurene FETs with Ag, Pt, Pd and graphene electrodes and a channel length of L = 5 nm. $\Phi_{L,T}^{e,a}$ ($\Phi_{L,T}^{e,b}$) and $\Phi_{L,T}^{h,a}$ ($\Phi_{L,T}^{h,b}$) represent the electron SBH and hole SBH in the lateral a (b) direction, respectively. The Fermi level is represented by the white and red dashed lines, respectively. MIGS are circled by a black dashed line. The color scale is shown below the plot.

Ohmic contact is formed with the graphene electrode in both a and b directions.

These two directions give nearly the same contact type and similar SBH, except for the Au electrode. A weak lateral n-type Schottky contact is formed in the a direction for the Au electrode, while a weak lateral p-type Schottky contact is formed in the b direction. This difference is because the Fermi level of the Au electrode is close to the band gap center of ML tellurene. Apparent MIGS are formed at the interface B (Fig. 5) for all the checked metals in both a and b directions and for the graphene electrode in the b direction, as shown in the black dashed irregular polygon in Fig. 6 and 7. In contrast, there are no MIGS at the interface B for graphene electrode in the a direction.

The lateral SBHs at the WFA level and the quantum transport simulation level in the a and b directions are compared in Fig. 8. These two methods give roughly the same contact

polarity, except for the Au electrode. The WFA method gives a lateral p-type Schottky contact for the Au electrode, while the quantum transport simulation only gives a lateral p-type Schottky contact in the *b* direction but a lateral n-type Schottky contact in the *a* direction. The WFA method tends to give a smaller lateral hole SBH or even an artificial lateral p-type Ohmic contact, while the quantum transport simulation tends to give a larger lateral hole SBH. These differences between the two methods suggest FLP at the interface between the metal electrodes and the channel, which is induced by the MIGS at the interface B.

For the graphene electrode, the WFA method gives a lateral p-type quasi-Ohmic contact with a very small hole SBH of 0.06 eV because the work function of the ML tellurene–graphene system (4.55 eV) is close to the VBM of intrinsic ML tellurene (4.61 eV). The quantum transport simulation gives a lateral p-type Ohmic contact for the graphene electrode in both *a* and *b* directions. The highly similar contact for the graphene electrode given by the two methods is attributed to the weak FLP originating from the absence of MIGS in the *a* direction and few MIGS in the *b* direction (Fig. 7).

Fig. 9(a) shows the lateral electron SBHs from the quantum transport simulation in the *a* direction and *b* direction as a function of the metal work functions. The slope, S, is defined as the FLP factor, which describes the degree of FLP. S = 1 represents no FLP and S = 0 implies complete pinning. A rather low FLP factor of S_a = 0.15 and S_b = 0.09 was obtained in the *a* direction and *b* direction, respectively, indicating strong FLP at the interface B and stronger FLP in the *b* direction than in the *a* direction. This FLP is illustrated more explicitly in Fig. 9(b), where the Fermi level is pinned from 0.3 eV below the CBM to the VBM of the ML tellurene. Both the FLP factors of ML tellurene are smaller than the theoretical S = 0.27 of ML MoS_2,[52] S = 0.28 of ML black phosphorene,[28] S = 0.33 of ML arsenene,[53,54] and S = 0.42 of ML blue phosphorene,[55] implying stronger FLP at interface B of ML tellurene.

Since the metals and ML graphene are stretched to match tellurene in our model, the SBHs will be affected by the work function change with the strain of the metals and ML graphene. To explore the effect of the lattice mismatch of the metals and ML graphene on the SBH, we chose Ni metal, which has the maximum mismatch in all the investigated metals, and ML graphene. On account of the strain, the work function varies from 5.08 to 5.01 eV for metal Ni and from 4.61 to 4.58 eV for ML graphene. These small changes indicate that the SBH only changes by 0.07 eV for metal Ni and 0.04 eV for ML graphene at the WFA level. On the other hand, the change in the SBH at the quantum transport simulation level is expected to be smaller than 0.07 eV for the metal Ni electrode and 0.04 eV for the ML graphene electrode due to the Fermi level pinning at the interface between the channel and the electrodes. Thus, the mismatch in our study has very slight effect on the SBHs in both methods.

The transport gap E_g^a (E_g^b) is defined as the sum of the lateral electron and hole SBH of $\Phi_{L,T}^{e,a}$ ($\Phi_{L,T}^{e,b}$) and $\Phi_{L,T}^{h,a}$ ($\Phi_{L,T}^{h,b}$) in the *a* (*b*) direction, that is, $E_g^a = \Phi_{L,T}^{e,a} + \Phi_{L,T}^{h,a}$ ($E_g^b = \Phi_{L,T}^{e,b} + \Phi_{L,T}^{h,b}$). The E_g^a (E_g^b) of the ML tellurene transistor with Sc, Au, Cu, Ni, Ag, Pt, Pd and graphene is 0.97, 0.98, 1.03, 0.99, 0.96, 0.97, 1.00 and 1.00 eV (0.98, 0.96, 1.02, 1.00, 1.00, 1.01, 0.97 and 0.97 eV), respectively, as listed in Table 1. E_g^a and E_g^b are close to each other and comparable with the band gap of the free-standing ML tellurene (1.14 eV).

Discussion

It was shown that ML black phosphorene prefers a lateral p-type Schottky contact with metals both experimentally and theoretically.[19,27] Our examination suggests that ML tellurene also prefers a lateral p-type Schottky contact with metal electrodes due to its small work function of 4.61 eV, which is comparable with the calculated value (4.57 eV) for ML black phosphorene.[28] In experiment, tellurene with a thickness of more than 5 nm

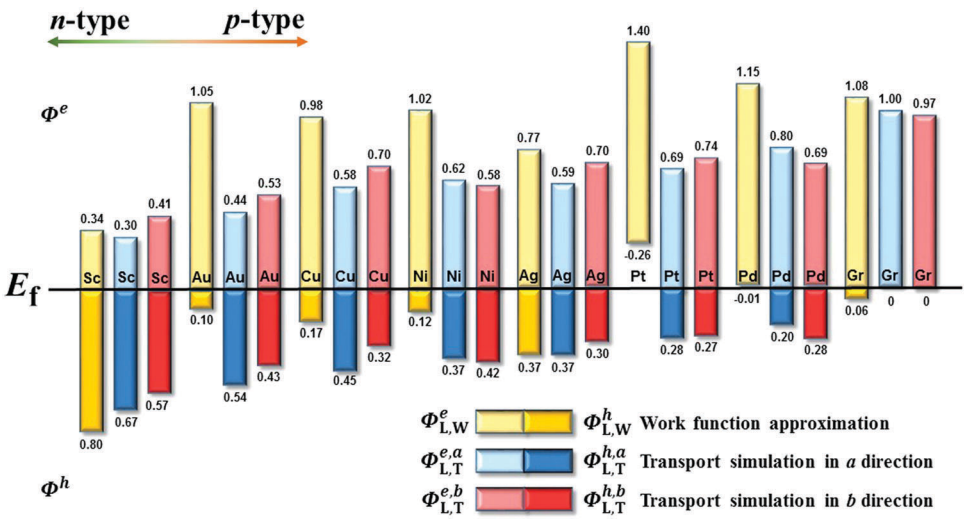

Fig. 8 Comparison of the lateral SBHs in the ML tellurene FET obtained from the work function approximation ($\Phi_{L,W}^{e/h}$) and the quantum transport simulation in the *a* ($\Phi_{L,T}^{e/h,a}$) direction and *b* ($\Phi_{L,T}^{e/h,b}$) direction.

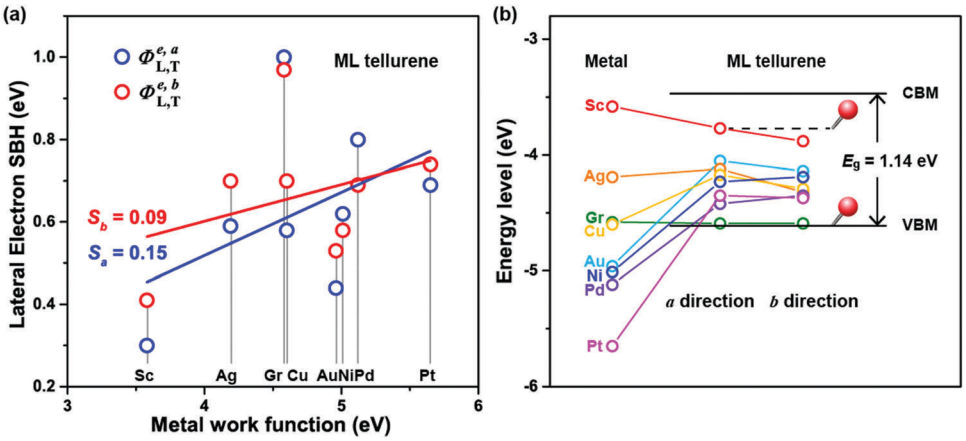

Fig. 9 (a) Comparison of the lateral electron SBH as a function of the metal work function in the *a* direction and *b* direction for the ML tellurene FETs. (b) Illustration of FLP in the ML tellurene transistor. *S* is the FLP factor.

forms a lateral p-type Ohmic contact with the Pd electrode,[6] while in our examination ML tellurene forms a lateral p-type Schottky contact. This difference is attributed to the fact that the band gap of tellurene decreases and the VBM of tellurene increases with an increase in the layer number, and thus a p-type Ohmic contact is favored in multilayer tellurene.

ML black phosphorene cannot form an Ohmic contact with common metal electrodes according to the quantum transport simulation, but a p-type Ohmic contact is formed with the graphene electrode.[28,56] Fortunately, in our examination, ML tellurene also forms a lateral p-type Ohmic contact with the graphene electrode in both directions despite the Schottky contact with the metal electrode. Hence graphene is the optimal electrode material for ML tellurene transistors, and a high performance is expected.

Conclusion

In summary, we provide comprehensive investigation of the interfacial properties of ML tellurene with bulk metal and 2D graphene electrodes using *ab initio* electronic structure calculations and quantum transport simulations. A lateral n-type Schottky contact is formed with the Sc electrode in both directions and Au electrode in the *a* direction. A lateral p-type Schottky contact is formed with the Cu, Ni, Ag, Pd and Pt electrodes in both directions and Au electrode in the *b* direction. The lateral Schottky barrier is caused by the strong FLP with the FLP factor S_a = 0.15 and S_b = 0.09, which is induced by MIGS at the interface B. Remarkably, ML tellurene forms a lateral p-type Ohmic contact with the graphene electrode in both directions owing to the match of the work function of ML graphene with the VBM of ML tellurene and weak FLP at the interface. Therefore, graphene is the optimal electrode material for ML tellurene transistors. Our systemic investigation provides a decent reference for the choice of an appropriate electrode in ML tellurene devices.

Conflicts of interest

There are no conflicts to declare.

Acknowledgements

This work was supported by the National Natural Science Foundation of China (No. 11274016/11474012/11674005/11274233/11664026), the National Basic Research Program of China (No. 2013CB932604/2012CB619304), the Ministry of Science and Technology (National Materials Genome Project) of China (No. 2016YFB0700600/2016YFA0301300). We would like to thank Prof. Peide D. Ye and Dr Gang Qiu for helpful discussions.

References

1 G. Fiori, F. Bonaccorso, G. Iannaccone, T. Palacios, D. Neumaier, A. Seabaugh, S. K. Banerjee and L. Colombo, Electronics Based on Two-dimensional Materials, *Nat. Nanotechnol.*, 2014, **9**(10), 768–779.
2 J. Kang, W. Liu, D. Sarkar, D. Jena and K. Banerjee, Computational Study of Metal Contacts to Monolayer Transition-Metal Dichalcogenide Semiconductors, *Phys. Rev. X*, 2014, **4**(3), 031005.
3 F. Schwierz, J. Pezoldt and R. Granzner, Two-dimensional Materials and Their Prospects inTransistor Electronics, *Nanoscale*, 2015, **7**(18), 8261–8283.
4 X. Huang, J. Guan, Z. Lin, B. Liu, S. Xing, W. Wang and J. Guo, Epitaxial Growth and Band Structure of Te Film on Graphene, *Nano Lett.*, 2017, **17**(8), 4619–4623.
5 Y. Du, G. Qiu, Y. Wang, M. Si, X. Xu, W. Wu and P. D. Ye, One-Dimensional van der Waals Material Tellurium: Raman Spectroscopy under Strain and Magneto-Transport, *Nano Lett.*, 2017, **17**(6), 3965–3973.
6 Y. Wang, G. Qiu, R. Wang, S. Huang, Q. Wang, Y. Liu, Y. Du, W. A. Goddard, M. J. Kim, X. Xu, P. D. Ye and W. Wu, Field-effect transistors made from solution-grown two-dimensional tellurene, *Nat. Electron.*, 2018, **1**(4), 228–236.
7 H. O. H. Churchill, G. J. Salamo, S. Q. Yu, T. Hironaka, X. Hu, J. Stacy and I. Shih, Toward Single Atom Chains with Exfoliated Tellurium, *Nanoscale Res. Lett.*, 2017, **12**, 6.

8 Z. Zhu, X. Cai, S. Yi, J. Chen, Y. Dai, C. Niu, Z. Guo, M. Xie, F. Liu, J. H. Cho, Y. Jia and Z. Zhang, Multivalency-Driven Formation of Te-Based Monolayer Materials: A Combined First-Principles and Experimental study, *Phys. Rev. Lett.*, 2017, **119**(10), 106101.

9 Z. Zhu; C. Cai; C. Niu; C. Wang; Q. Sun and Y. Jia Tellurene-a Monolayer of Tellurium from First-principles Prediction, 2016, arXiv:1605.03253.

10 A. Coker, T. Lee and T. P. Das, Investigation of the Electronic-properties of Tellurium-energy-band Structure, *Phys. Rev. B: Condens. Matter Mater. Phys.*, 1980, **22**(6), 2968–2975.

11 A. Vonhippel, Structure and Conductivity in the VIB Group of the Periodic System, *J. Chem. Phys.*, 1948, **16**(4), 372–380.

12 V. B. Anzin, M. I. Eremets, Y. V. Kosichkin, A. I. Nadezhdinskii and A. M. Shirokov, Measurement of Energy-gap in Tellurium under Pressure, *Phys. Status Solidi A*, 1977, **42**(1), 385–390.

13 P. Cherin and P. Unger, 2-dimensional Refinement of Crystal Structure of Tellurium, *Acta Crystallogr.*, 1967, **23**, 670.

14 S. Kim, A. Konar, W. S. Hwang, J. H. Lee, J. Lee, J. Yang, C. Jung, H. Kim, J. B. Yoo, J. Y. Choi, Y. W. Jin, S. Y. Lee, D. Jena, W. Choi and K. Kim, High-Mobility and Low-power Thin-film Transistors Based on Multilayer MoS_2 Crystals, *Nat. Commun.*, 2012, **3**, 7.

15 W. Z. Bao, X. H. Cai, D. Kim, K. Sridhara and M. S. Fuhrer, High Mobility Ambipolar MoS_2 Field-effect Transistors: Substrate and Dielectric Effects, *Appl. Phys. Lett.*, 2013, **102**(4), 4.

16 D. Jariwala, V. K. Sangwan, D. J. Late, J. E. Johns, V. P. Dravid, T. J. Marks, L. J. Lauhon and M. C. Hersam, Band-like Transport in High Mobility Unencapsulated Single-layer MoS_2 Transistors, *Appl. Phys. Lett.*, 2013, **102**(17), 4.

17 S. Larentis, B. Fallahazad and E. Tutuc, Field-effect Transistors and Intrinsic Mobility in Ultra-thin $MoSe_2$ Layers, *Appl. Phys. Lett.*, 2012, **101**(22), 4.

18 B. Chamlagain, Q. Li, N. J. Ghimire, H. J. Chuang, M. M. Perera, H. G. Tu, Y. Xu, M. Pan, D. Xaio, J. Q. Yan, D. Mandrus and Z. X. Zhou, Mobility Improvement and Temperature Dependence in $MoSe_2$ Field-Effect Transistors on Parylene-C Substrate, *ACS Nano*, 2014, **8**(5), 5079–5088.

19 N. R. Pradhan, D. Rhodes, Y. Xin, S. Memaran, L. Bhaskaran, M. Siddiq, S. Hill, P. M. Ajayan and L. Balicas, Ambipolar Molybdenum Diselenide Field-Effect Transistors: Field-Effect and Hall Mobilities, *ACS Nano*, 2014, **8**(8), 7923–7929.

20 X. L. Wang, Y. J. Gong, G. Shi, W. L. Chow, K. Keyshar, G. L. Ye, R. Vajtai, J. Lou, Z. Liu, E. Ringe, B. K. Tay and P. M. Ajayan, Chemical Vapor Deposition Growth of Crystalline Mono layer $MoSe_2$, *ACS Nano*, 2014, **8**(5), 5125–5131.

21 L. K. Li, Y. J. Yu, G. J. Ye, Q. Q. Ge, X. D. Ou, H. Wu, D. L. Feng, X. H. Chen and Y. B. Zhang, Black Phosphorus Field-effect Transistors, *Nat. Nanotechnol.*, 2014, **9**(5), 372–377.

22 H. Liu, A. T. Neal, Z. Zhu, Z. Luo, X. Xu, D. Tomanek and P. D. Ye, Phosphorene: An Unexplored 2D Semiconductor with a High Hole Mobility, *ACS Nano*, 2014, **8**(4), 4033–4041.

23 H. Liu, Y. C. Du, Y. X. Deng and P. D. Ye, Semiconducting Black Phosphorus: Synthesis, Transport Properties and Electronic Applications, *Chem. Soc. Rev.*, 2015, **44**(9), 2732–2743.

24 A. Allain, J. H. Kang, K. Banerjee and A. Kis, Electrical Contacts to Two-dimensional Semiconductors, *Nat. Mater.*, 2015, **14**(12), 1195–1205.

25 S. Das, M. Demarteau and A. Roelofs, Ambipolar Phosphorene Field Effect Transistor, *ACS Nano*, 2014, **8**(11), 11730–11738.

26 S. Das, W. Zhang, M. Demarteau, A. Hoffmann, M. Dubey and A. Roelofs, Tunable Transport Gap in Phosphorene, *Nano Lett.*, 2014, **14**(10), 5733–5739.

27 Y. Wang, P. Huang, M. Ye, R. Quhe, Y. Pan, H. Zhang, H. Zhong, J. Shi and J. Lu, Many-body Effect, Carrier Mobility, and Device Performance of Hexagonal Arsenene and Antimonene, *Chem. Mater.*, 2017, **29**(5), 2191–2201.

28 Y. Pan, Y. Wang, M. Ye, R. Quhe, H. Zhong, Z. Song, X. Peng, D. Yu, J. Yang, J. Shi and J. Lu, Monolayer Phosphorene-Metal Contacts, *Chem. Mater.*, 2016, **28**(7), 2100–2109.

29 Y. Pan, S. Li, M. Ye, R. Quhe, Z. Song, Y. Wang, J. Zheng, F. Pan, W. Guo, J. Yang and J. Lu, Interfacial Properties of Monolayer $MoSe_2$-Metal Contacts, *J. Phys. Chem. C*, 2016, **120**(24), 13063–13070.

30 J. H. Kang, W. Liu, D. Sarkar, D. Jena and K. Banerjee, Computational Study of Metal Contacts to Monolayer Transition-Metal DichalcogenideSemiconductors, *Phys. Rev. X*, 2014, **4**(3), 031005.

31 J. Zheng, Y. Wang, L. Wang, R. Quhe, Z. Ni, W.-N. Mei, Z. Gao, D. Yu, J. Shi and J. Lu, Interfacial Properties of Bilayer and Trilayer Graphene on Metal Substrates, *Sci. Rep.*, 2013, **3**, 2081.

32 G. Kresse and D. Joubert, From Ultrasoft Pseudopotentials to the Projector Augmented-wave Method, *Phys. Rev. B: Condens. Matter Mater. Phys.*, 1999, **59**, 1758–1775.

33 P. E. Blöchl, Projector Augmented-wave Method, *Phys. Rev. B: Condens. Matter Mater. Phys.*, 1994, **50**(24), 17953–17979.

34 G. Kresse and J. Hafner, *Ab-initio* Molecular-Dynamics For Liquid-Metals, *Phys. Rev. B: Condens. Matter Mater. Phys.*, 1993, **47**(1), 558–561.

35 G. Kresse and J. Hafner, *Ab-initio* Molecular-Dynamic Simulation of the Liquid-Metal Amorphous-Semiconductor Transition in Germanium, *Phys. Rev. B: Condens. Matter Mater. Phys.*, 1994, **49**(20), 14251–14269.

36 G. Kresse and J. Furthmuller, Efficiency of *Ab-initio* Total Energy Calculations for Metals and Semiconductors Using a Plane-wave Basis Set, *Comput. Mater. Sci.*, 1996, **6**(1), 15–50.

37 G. Kresse and J. Furthmuller, Efficient Iterative Schemes for *Ab initio* Total-energy Calculations Using a Plane-wave Basis Set, *Phys. Rev. B: Condens. Matter Mater. Phys.*, 1996, **54**(16), 11169–11186.

38 H. J. Monkhorst and J. D. Pack, Special Points For Brillouin-Zone Integrations, *Phys. Rev. B: Condens. Matter Mater. Phys.*, 1976, **13**(12), 5188–5192.

39 S. Grimme, J. Antony, S. Ehrlich and H. Krieg, A consistent and accurate *ab initio* parametrization of density functional dispersion correction (DFT-D) for the 94 elements H–Pu, *J. Chem. Phys.*, 2010, **132**(15), 19.

40 Y. Yuan, R. Quhe, J. Zheng, Y. Wang, Z. Ni, J. Shi and J. Lu, Strong Band Hybridization between Silicene and Ag(111) Substrate, *Physica E*, 2014, **58**, 38–42.

41 M. Brandbyge, J. L. Mozos, P. Ordejon, J. Taylor and K. Stokbro, Density-functional Method for Nonequilibrium Electron Transport, *Phys. Rev. B: Condens. Matter Mater. Phys.*, 2002, **65**(16), 165401.

42 Atomistix ToolKit, version 2016; QuantumWise A/S: Copenhagen, Denmark, 2017. http://www.quantumwise.com (accessed Jun 9, 2017).

43 J. M. Soler, E. Artacho, J. D. Gale, A. Garcia, J. Junquera, P. Ordejon and D. Sanchez-Portal, The SIESTA Method for *Ab Initio* Order-N Materials Simulation, *Phys. Rev. B: Condens. Matter Mater. Phys.*, 2002, **14**(11), 2745–2779.

44 D. R. Smith, S. Schultz, P. Markos and C. M. Soukoulis, Determination of Effective Permittivity and Permeability of Metamaterials from Reflection and Transmission Coefficients, *Phys. Rev. B: Condens. Matter Mater. Phys.*, 2002, **65**(19), 5.

45 D. Cakir and F. M. Peeters, Dependence of the Electronic and Transport Properties of Metal–$MoSe_2$ Interfaces on Contact Structures, *Phys. Rev. B: Condens. Matter Mater. Phys.*, 2014, **89**(24), 7.

46 A. H. D. Cheng and D. T. Cheng, Heritage and Early History of the Boundary Element Method, *Eng. Anal. Bound Elem.*, 2005, **29**(3), 268–302.

47 J. P. Perdew, K. Burke and M. Ernzerhof, Generalized Gradient Approximation Made Simple, *Phys. Rev. Lett.*, 1996, **77**(18), 3865–3868.

48 R. Quhe, R. Fei, Q. Liu, J. Zheng, H. Li, C. Xu, Z. Ni, Y. Wang, D. Yu, Z. Gao and J. Lu, Tunable and Sizable Band Gap in Silicene by Surface Adsorption, *Sci. Rep.*, 2012, **2**, 853.

49 Y. Liang and L. Yang, Carrier Plasmon Induced Nonlinear Band Gap Renormalization in Two-dimensional Semiconductors, *Phys. Rev. Lett.*, 2015, **114**(6), 063001.

50 Y. Pan, Y. Dan, Y. Wang, M. Ye, H. Zhang, R. Quhe, X. Zhang, J. Li, W. Guo, L. Yang and J. Lu, Schottky Barriers in Bilayer Phosphorene Transistors, *ACS Appl. Mater. Interfaces*, 2017, **9**(14), 12694–12705.

51 X. Zhang, Y. Pan, M. Ye, R. Quhe, Y. Wang, Y. Guo, H. Zhang, Y. Dan, Z. Song, J. Li, J. Yang, W. Guo and J. Lu, Three-layer Phosphorene-metal Interfaces, *Nano Res.*, 2018, **11**(2), 707–721.

52 H. Zhong, R. Quhe, Y. Wang, Z. Ni, M. Ye, Z. Song, Y. Pan, J. Yang, L. Yang, M. Lei, J. Shi and J. Lu, Interfacial Properties of Monolayer and Bilayer MoS_2 Contacts with Metals: Beyond the Energy Band Calculations, *Sci. Rep.*, 2016, **6**, 21786.

53 Y. Wang, M. Ye, M. Weng, J. Li, X. Zhang, H. Zhang, Y. Guo, Y. Pan, L. Xiao, J. Liu, F. Pan and J. Lu, Electrical Contacts in Monolayer Arsenene Devices, *ACS Appl. Mater. Interfaces*, 2017, **9**(34), 29273–29284.

54 Y. Guo, D. Liu and J. Robertson, 3D Behavior of Schottky Barriers of 2D Transition-Metal Dichalcogenides, *ACS Appl. Mater. Interfaces*, 2015, **7**(46), 25709–25715.

55 J. Li, X. Sun, C. Xu, X. Zhang, Y. Pan, M. Ye, Z. Song, R. Quhe, Y. Wang, H. Zhang, Y. Guo, J. Yang, F. Pan and J. Lu, Electrical contacts in monolayer blue phosphorene devices, *Nano Res.*, 2018, **11**(4), 1834–1849.

56 R. Quhe, X. Peng, Y. Pan, M. Ye, Y. Wang, H. Zhang, S. Feng, Q. Zhang, J. Shi, J. Yang, D. Yu, M. Lei and J. Lu, Can a Black Phosphorus Schottky Barrier Transistor Be Good Enough?, *ACS Appl. Mater. Interfaces*, 2017, **9**(4), 3959–3966.